Diffraction of electrons at intermediate energies

H. Ascolani, R. O. Barrachina, M. M. Guraya, and G. Zampieri
Centro Atómico Bariloche, Comisión Nacional de Energía Atómica, 8400 San Carlos de Bariloche, Argentina
(Received 22 October 1991; revised manuscript received 27 March 1992)

We present a theory of the elastic scattering of electrons from crystalline surfaces that contains both low-energy-electron-diffraction (LEED) effects at low energies and x-ray-photoelectron- and Auger-electron-diffraction (XPD/AED) effects at intermediate energies. The theory is based on a cluster-type approach to the scattering problem and includes temperature effects. The transition from one regime to the other may be explained as follows: At low energies all the scattered waves add coherently, and the intensity is dominated by LEED effects. At intermediate energies the thermal vibration of the atoms destroys the long-range coherency responsible for the LEED peaks, but affects little the interference of those waves that share parts of their paths inside the solid. Thus, the interference of these waves comes to dominate the intensity, giving rise to structures similar to those observed in XPD/AED experiments. We perform a calculation of the elastic reflection of electrons from Cu(001) that is in good agreement with the experiment in the range 200–1500 eV. At low energies the intensity is dominated by LEED peaks; at 400 eV LEED peaks and XPD/AED structures coexist; and above this energy the intensity is dominated by the latter. We analyze the contributions to the intensity at intermediate energies of the interferences in the incoming and outgoing parts of the electron path.

I. INTRODUCTION

It is now well established that x-ray photoelectron diffraction (XPD), Auger electron diffraction (AED), and angle-resolved photoemission extended fine structure (ARPEFS) can yield accurate information on the local geometric structure of crystalline surfaces.[1–4] In XPD and AED the intensity of an Auger or core-level photoelectron line is studied as a function of the emission direction; it is seen that the focusing of the outgoing electron by the attractive potential of the near neighbors of the emitting atom produces strong peaks at the internuclear directions. In ARPEFS the emission direction is kept fixed and the intensity of a core-level peak is studied as a function of the photon energy; the fine-structure modulations are due to the interference between the *direct* photoelectron wave and the *secondary* waves produced by the scattering with the neighboring atoms.

Some applications of these ideas to the problem of the elastic and quasielastic reflection of electrons from crystalline surfaces have recently appeared in the literature. While Barton, Xu, and Van Hove[5] have formulated a cluster-type theory of low-energy electron diffraction (LEED) that offers a new perspective on the electron-diffraction problem, other authors[6–8] have concentrated on the patterns observed at energies of several hundred electron volts, which are very similar to those observed in XPD and AED.

We present in this work a theory of the elastic reflection of electrons from crystalline surfaces that contains both the LEED effects at low energies and the XPD/AED effects at medium energies. The theory follows the treatment of Ref. 5, but includes the thermal vibration of the atoms, which, as will be shown below, is the key ingredient to describe the transition from one regime to the other. The paper is organized as follows: The experiment and the theory are described in Secs. II and III, respectively, and compared in Sec. IV. Some aspects of the transition from the LEED to the AED/XPD regime and future improvements of the theoretical model are discussed in Sec. V. Finally, our main results are summarized in Sec. VI.

II. EXPERIMENT

The experiment has been described in detail in Ref. 8. We measured the intensity of the elastic reflection of electrons impinging on Cu(001) as a function of the polar angle of emergence along the [010] azimuth and of the electron energy. A schematic drawing of the experimental geometry is shown in Fig. 1.

All the measurements were performed in an UHV chamber operated at a base pressure of 10^{-10} Torr. The

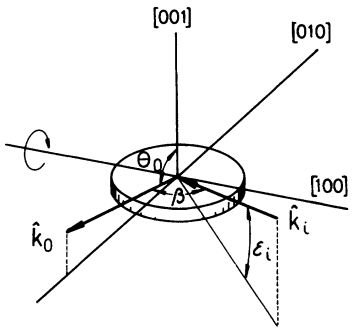

FIG. 1. Schematic illustration of the experimental geometry. When the sample is rotated on the [100] axis, both the polar angle of the scattered electrons, θ_0, and the elevation angle of the incident beam, ϵ_i, change; the scattering angle π-β remains constant at 144.35°. For $\theta_0=75°$ the elevation angle is $\epsilon_i=30°$.

electron spectrometer was a 150° spherical sector analyzer with a preretarding grid; it was operated in the constant retard ratio mode giving an energy resolution $\Delta E/E=0.5\%$. The angular resolution was found to be $\pm 6°$.

The sample, a Cu(001) single-crystal disc of 6 mm diameter, was mechanically polished with alumina of 0.05 μm. A clean and ordered crystal surface was obtained after repeated cycles of Ar bombardment and annealing at 800 K in vacuum.

The intensity of the elastic scattering from polycrystalline Cu was also measured, and used to normalize the results obtained with the crystal.

III. THEORY

A. The scattering problem at $T=0$

We shall consider the elastic scattering of a plane wave with wave vector $\mathbf{k}_i$ by a perfect crystal with the atoms fixed at their rest positions. Following the treatment of Ref. 5, the atom potentials will be represented by spherically symmetrical muffin-tin potentials and the total scattered wave will be expanded in terms of individual scattering events in the following way:

$$\psi_s(\mathbf{r})=\sum_n \psi_n(\mathbf{r})+\sum_n \sum_{l\neq n} \psi_{nl}(\mathbf{r})+\sum_n \sum_{l\neq n} \sum_{j\neq l} \psi_{nlj}(\mathbf{r})+\cdots ,$$

where $\psi_n(\mathbf{r})$ is the wave produced by the scattering of the plane wave by the atom at position $\mathbf{R}_n$, $\psi_{nl}(\mathbf{r})$ is the wave produced by the scattering of ψ_n by the atom at position $\mathbf{R}_l$, and so on.

$\psi_n(\mathbf{r})$ is the familiar scattered wave of a plane wave incident on a central potential; if the detector is far away from the surface, at position $\mathbf{R}$, ψ_n can be written as

$$\psi_n(\mathbf{R})=A_n \frac{\exp(ikR)}{R}$$

with

$$A_n=f(\theta_{i,o})\exp[i(\mathbf{k}_i-\mathbf{k}_o)\cdot\mathbf{R}_n] ,$$

where $k=|\mathbf{k}_i|$, $\mathbf{k}_o=k\hat{\mathbf{R}}$, $\theta_{i,o}$ is the angle between $\mathbf{k}_i$ and $\mathbf{k}_o$, and $f(\theta)$ is the elastic scattering amplitude.

$\psi_{nl}(\mathbf{r})$ corresponds to the scattering of the *spherical* wave ψ_n by the atom at $\mathbf{R}_l$. In the *plane-wave* approximation,[9] ψ_{nl} at the detector position can be written as

$$\psi_{nl}(\mathbf{R})=A_{nl}\frac{\exp(ikR)}{R}$$

with

$$A_{nl}=f(\theta_{i,ln})\exp[i(\mathbf{k}_i-\mathbf{k}_{ln,o})\cdot\mathbf{R}_n]\frac{1}{R_{ln}}f(\theta_{ln,o}) \times\exp[i(\mathbf{k}_{ln}-\mathbf{k}_o)\cdot\mathbf{R}_l] ,$$

where $\mathbf{k}_{ln}=k\hat{\mathbf{R}}_{ln}$, with $\mathbf{R}_{ln}=\mathbf{R}_l-\mathbf{R}_n$, and $\theta_{i,ln}$ ($\theta_{ln,o}$) is the angle between $\mathbf{k}_i$ ($\mathbf{k}_o$) and $\mathbf{k}_{ln}$.

Higher-order waves can also be written as a spherical wave times an amplitude, and this latter can be built by inspection; for example, the amplitude A_{nl} can be read as follows: (i) for each scattering event there is a product of the scattering amplitude times a phase factor formed with the change of wave vector and the atom position, and (ii) for each pair of consecutive scattering events at $\mathbf{R}_n$ and $\mathbf{R}_l$ there is a $1/R_{ln}$ factor.

The total scattered wave at the detector can now be written as

$$\psi_s(\mathbf{R})=\left[\sum_n A_n\exp(-L_n/2\lambda) + \sum_n \sum_{l\neq n} A_{nl}\exp(-L_{nl}/2\lambda)+\cdots\right]\frac{\exp(ikR)}{R} , \tag{1}$$

where the effect of the inelastic collisions has been introduced by weighting each amplitude with an attenuation factor $\exp(-L/2\lambda)$, with L the total electron path inside the solid and λ the electron mean free path. Finally, the intensity at the detector is given by the square modulus of ψ_s and can be expressed as

$$I(\mathbf{k}_i,\mathbf{k}_o)=\frac{1}{R^2}\sum_n \sum_{n'} A_n A_{n'}^* \exp[-(L_n+L_{n'})/2\lambda] + \frac{2}{R^2}\mathrm{Re}\sum_n \sum_{l\neq n} \sum_{n'} A_{nl} A_{n'}^* \times\exp[-(L_{nl}+L_{n'})/2\lambda] + \cdots . \tag{2}$$

The first term on the right-hand side of Eq. (2) corresponds to the interference between singly scattered waves (SSW's), and the second term to the interference between doubly scattered waves (DSW's) and SSW's; omitted are the terms corresponding to the interferences between DSW's and between SSW's and triply scattered waves (same order in the number of scattering events), and to all higher-order interferences. In the interest of mathematical simplicity we will keep in what follows only those terms explicitly written in (2).

B. The effect of the temperature

The above expression for the intensity at $T=0$ is totally equivalent to that derived in Ref. 5, except for our use of the plane-wave approximation. To include now the thermal vibration of the atoms we proceed in the usual way;[10] since the time scale on which the electron scattering occurs is much shorter than the characteristic periods of the atomic oscillations, we assume that during the scattering the crystal is frozen with the atoms at positions $\mathbf{R}_n=\mathbf{R}_n^0+\mathbf{u}_n$, where $\mathbf{R}_n^0$ is the equilibrium position and $\mathbf{u}_n$ the displacement vector. Using $\mathbf{R}_n^0+\mathbf{u}_n$ in the phase factors of the amplitudes A_n and A_{nl} one obtains an expression for the *instantaneous* intensity. The *observed* intensity is the average of the *instantaneous* intensity over the displacements $\mathbf{u}_n$; this involves the calculation of the averages:

$$P_{n,n'}=\langle\exp[i(\mathbf{k}_i-\mathbf{k}_o)\cdot\mathbf{u}_n-i(\mathbf{k}_i-\mathbf{k}_o)\cdot\mathbf{u}_{n'}]\rangle \tag{3}$$

and

$$P_{nl,n'}=\langle \exp[i(\mathbf{k}_i-\mathbf{k}_{ln})\cdot\mathbf{u}_n+i(\mathbf{k}_{ln}-\mathbf{k}_o)\cdot\mathbf{u}_l-i(\mathbf{k}_i-\mathbf{k}_o)\cdot\mathbf{u}_{n'}]\rangle \ . \tag{4}$$

Use of the formula[11]

$$\langle \exp(i\,\mathbf{A}\cdot\mathbf{u}_n+i\mathbf{B}\cdot\mathbf{u}_{n'})\rangle=\exp[-\tfrac{1}{2}\langle(\mathbf{A}\cdot\mathbf{u}_n+\mathbf{B}\cdot\mathbf{u}_{n'})^2\rangle]$$

reduces the problem to calculating the average in the argument of the second exponential, and assuming that the atomic vibrations are *isotropic* and *uncorrelated* one obtains

$$\langle(\mathbf{A}\cdot\mathbf{u}_n)^2\rangle=|\mathbf{A}|^2\langle u_z^2\rangle=|\mathbf{A}|^2\sigma^2 \ , \tag{5}$$

$$\langle(\mathbf{A}\cdot\mathbf{u}_n)(\mathbf{B}\cdot\mathbf{u}_{n'})\rangle=\delta_{nn'}(\mathbf{A}\cdot\mathbf{B})\langle u_z^2\rangle=\delta_{nn'}(\mathbf{A}\cdot\mathbf{B})\sigma^2 \ . \tag{6}$$

Finally, using Eqs. (5) and (6) to compute the thermal averages (3) and (4), one obtains the following expression for the *observed* intensity:

$$\begin{aligned}\langle I(\mathbf{k}_i,\mathbf{k}_o)\rangle=&\frac{1}{R^2}\sum_n\sum_{n'}A_nA_{n'}^*F^{(0)}\exp[-(L_n+L_{n'})/2\lambda]+\frac{2}{R^2}\mathrm{Re}\sum_n\sum_{l\neq n}\sum_{n'}A_{nl}A_{n'}^*F_{nl}^{(0)}\exp[-(L_{nl}+L_{n'})/2\lambda]\\&+\frac{1}{R^2}\sum_n|A_n|^2(1-F^{(0)})\exp(-L_n/\lambda)\\&+\frac{2}{R^2}\mathrm{Re}\sum_n\sum_{l\neq n}A_{nl}A_n^*(F_{nl}^{(1)}-F_{nl}^{(0)})\exp[-(L_{nl}+L_n)/2\lambda]\\&+\frac{2}{R^2}\mathrm{Re}\sum_n\sum_{l\neq n}A_{nl}A_l^*(F_{nl}^{(2)}-F_{nl}^{(0)})\exp[-(L_{nl}+L_l)/2\lambda] \ ,\end{aligned} \tag{7}$$

where $F^{(0)}$, $F_{nl}^{(0)}$, $F_{nl}^{(1)}$, and $F_{nl}^{(2)}$ are Debye-Waller factors defined as follows:

$$F^{(0)}=\exp(-|\mathbf{k}_i-\mathbf{k}_o|^2\sigma^2) \ ,$$

$$F_{nl}^{(0)}=\exp[-\tfrac{1}{2}(|\mathbf{k}_i-\mathbf{k}_{ln}|^2+|\mathbf{k}_{ln}-\mathbf{k}_o|^2+|\mathbf{k}_i-\mathbf{k}_o|^2)\sigma^2] \ ,$$

$$F_{nl}^{(1)}=\exp(-|\mathbf{k}_o-\mathbf{k}_{ln}|^2\sigma^2) \ ,$$

$$F_{nl}^{(2)}=\exp(-|\mathbf{k}_i-\mathbf{k}_{ln}|^2\sigma^2) \ .$$

The first term on the right-hand side of Eq. (7) is the result of the single-scattering or kinematic model of LEED, and the second term is the first-order correction of this model. We shall group these two terms in I_{LEED}; they represent the *coherent* part of the scattering. The third term corresponds to the thermal diffuse background in the kinematic model; we shall call it I_{dif}. The fourth and fifth terms will be named I_{inc} and I_{out}, respectively, for reasons which will become clear in the next section. Following the usual terminology, we shall consider that the last three terms, I_{dif}, I_{inc}, and I_{out}, represent the *incoherent* part of the scattering, although, as we shall demonstrate below, a high degree of *coherency* is still present.

Note that none of the terms defined above needs to be positive; only the sum represents an intensity and should always be positive. However, as we have neglected the contribution of the interference between DSW's, even the sum may result in some cases slightly negative. In spite of the nonseparability of the terms, it can certainly be expected that I_{LEED} and the sum $I_{\mathrm{inc}}+I_{\mathrm{out}}+I_{\mathrm{dif}}$ behave as the coherent and incoherent "intensities," respectively, taking always positive values. We will show that this is indeed so, and that the incoherent intensity behaves as the intensity in XPD/AED experiments: strong modulations, due to the terms I_{inc} and I_{out}, appear superimposed on the smooth background provided by the term I_{dif}.

C. Analysis of the intensity terms

In this section we will analyze briefly the main properties of the terms I_{LEED} and I_{dif}, and in more detail those of the new terms I_{inc} and I_{out}.

1. I_{LEED}

This term corresponds to the coherent part of the intensity. It is formed with the products of the amplitudes of the waves shown in Fig. 2(a), and accounts for all the intensity at $T=0$. Barton, Xu, and Van Hove[5] have recently discussed the main features of this intensity at $T=0$ and in the regime of intermediate energies. At $T\neq 0$ the structure of the term is preserved with the products of wave amplitudes being weighted with the Debye-Waller (DW) factors $F^{(0)}$ and $F_{nl}^{(0)}$. These DW factors are determined essentially by the change of wave vector $\mathbf{k}_i-\mathbf{k}_o$, and for most backscattering geometries decrease rapidly when the temperature and/or the energy are increased; this is shown in Fig. 3 for $\theta_{i,o}=144°$.

2. I_{dif}

This term is formed with the square moduli of the SSW's, as shown in Fig. 2(b).[12] Clearly the square modulus of a wave is unaffected by the thermal motion of the atoms of the crystal. Then, this kind of product has been incorrectly attenuated with the DW factor $F^{(0)}$ in I_{LEED}, and I_{dif} "corrects" this by summing them weighted with the factor $1-F^{(0)}$. This term is negligible at low temperatures but becomes increasingly important as the

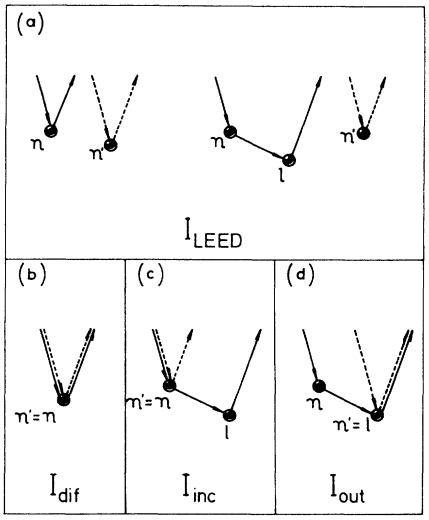

FIG 2. Schematic illustration of electron paths whose interferences contribute to the intensity terms I_{LEED}, I_{dif}, I_{inc}, and I_{out}. In (b) the waves have the same paths; in (c) the *incoming* paths are equal, and in (d) the *outgoing* paths are equal.

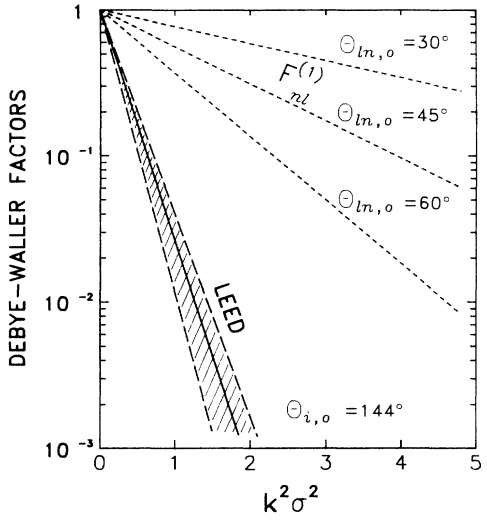

FIG. 3. Debye-Waller factors of the intensity terms I_{LEED} and I_{inc}. The full line corresponds to $F^{(0)}$, the long-dashed lines to the maximum and minimum $F_{nl}^{(0)}$, and the dashed lines to $F_{nl}^{(1)}$ for three angles between $\mathbf{R}_{ln}$ and $\mathbf{k}_o$.

temperature and/or the energy are increased and eventually dominates all the intensity.

3. I_{inc} and I_{out}

Figures 2(c) and 2(d) show the pairs of waves whose products give rise to the terms I_{inc} and I_{out}. Defining the *incoming* and *outgoing* paths of a wave as the path from the electron gun to the first scatterer and the path from the last scatterer to the detector, we may say that I_{inc} and I_{out} are formed with the interferences of waves with the same incoming or outgoing paths, respectively.

The two waves represented in Fig. 2(c) reach the atom at $\mathbf{R}_n$ with exactly the same phase, irrespective of the thermal motion of the atom; since no phase difference is accumulated in the incoming paths, the interference is of the same type as those found in XPD/AED and ARPEFS. These interferences are much less affected by the temperature than the general interferences considered in I_{LEED}; in particular, they are not weighted with DW factors $F_{nl}^{(0)}$ but with DW factors $F_{nl}^{(1)}$, which are determined by the change of wave vector $\mathbf{k}_o-\mathbf{k}_{ln}$ and may decay with the temperature and/or the energy very slowly if the exit direction $\hat{\mathbf{k}}_o$ falls near to an internuclear direction. This effect is illustrated in Fig. 3.

Conversely, for the two waves shown in Fig. 2(d), no phase difference is accumulated in the outgoing paths and the interference becomes independent of $\mathbf{k}_o$. Again, the interferences of this kind are much less affected by the temperature than those considered in I_{LEED}, and are weighted with DW factors $F_{nl}^{(2)}$, which depend only on the change of wave vector $\mathbf{k}_i-\mathbf{k}_{ln}$, instead of $F_{nl}^{(0)}$. Similarly to $F_{nl}^{(1)}$, the DW factors $F_{nl}^{(2)}$ may decay very slowly with the temperature and/or the energy if the incoming direction $\hat{\mathbf{k}}_i$ falls near to an internuclear direction.

Note that these intensity terms are different from those defined in Ref. 5. This is not surprising as we have used different criteria: while Barton, Xu, and Van Hove have grouped the interferences by the type of phase difference between the waves, we have grouped them by the type of thermal attenuation. Another important difference is that the analysis of Ref. 5 is based on the assumption that the two-dimensional (2D) Bragg conditions are met, whereas this is not used in our analysis. A comparison of the terms assuming that the 2D Bragg conditions are met shows that I_{inc} is contained in the term I_{ARPEFS} of Ref. 5, and that a part of I_{out} is contained in I_{ARPEFS} (that part due to interferences in which the atoms are in the same layer) and another in I_{comb} (when the atoms are in different layers).

There is a high symmetry between the terms I_{inc} and I_{out}. This is made more evident if one compares their explicit forms

$$I_{\mathrm{inc}}=\frac{2}{R^2}\mathrm{Re}\left[f(\theta_{i,o})^*\sum_n\sum_{l\neq n}\frac{f(\theta_{i,ln})f(\theta_{ln,o})}{R_{ln}}\exp[-(L_{nl}+L_n)/2\lambda](F_{nl}^{(1)}-F_{nl}^{(0)})\exp[ikR_{ln}(1-\cos\theta_{ln,o})]\right],$$

$$I_{\mathrm{out}}=\frac{2}{R^2}\mathrm{Re}\left[f(\theta_{i,o})^*\sum_n\sum_{l\neq n}\frac{f(\theta_{i,ln})f(\theta_{ln,o})}{R_{ln}}\exp[-(L_{nl}+L_l)/2\lambda]\times(F_{nl}^{(2)}-F_{nl}^{(0)})\exp[ikR_{ln}(1-\cos\theta_{i,ln})]\right].$$

It can be proven that these terms satisfy the following relationship:

$$I_{\text{out}}(\mathbf{k}_i,\mathbf{k}_o)=I_{\text{inc}}(-\mathbf{k}_o,-\mathbf{k}_i)\ ,$$

which expresses that the term I_{out} is the same as the term I_{inc} when the motion is reversed, i.e., when the plane wave impinges along $-\hat{\mathbf{k}}_o$ and the detector is along $-\hat{\mathbf{k}}_i$. Notice that when the motion is reversed both terms I_{inc} and I_{out} change, but the sum $I_{\text{inc}}+I_{\text{out}}$ is conserved.

Another important feature of these terms is that for a given first scatterer of the DSW, the main contributions to I_{inc} correspond to those second scatterers located inside a cone around the exit direction $\hat{\mathbf{k}}_o$, whereas the main contributions to I_{out} come from those second scatterers located inside a cone around the incoming direction $\hat{\mathbf{k}}_i$. This is due to the combined action of the elastic scattering amplitude, which is strongly peaked in the forward direction at intermediate energies, and the DW factors $F_{nl}^{(1)}$ and $F_{nl}^{(2)}$, which are maximum when $\mathbf{k}_{ln}$ is parallel to $\mathbf{k}_o$ or $\mathbf{k}_i$, respectively. Figure 4 shows these effects for a scattering problem in 2D. In Fig. 4(a) we have plotted in polar coordinates the DW factor $F_{nl}^{(1)}$ and the product of the scattering amplitudes $f(\theta_{i,ln})f(\theta_{ln,o})$. The product of the scattering amplitudes has prominent peaks in both the incoming and outgoing directions, but the DW factor $F_{nl}^{(1)}$ selects only one of them, namely, the one along $\hat{\mathbf{k}}_o$. Figure 4(b) shows that the final result is a single lobe directed along the outgoing direction. Figures 4(c) and 4(d) show that the product of the scattering amplitudes weighted with the DW factor $F_{nl}^{(2)}$ is again a single lobe, but directed along $\hat{\mathbf{k}}_i$.

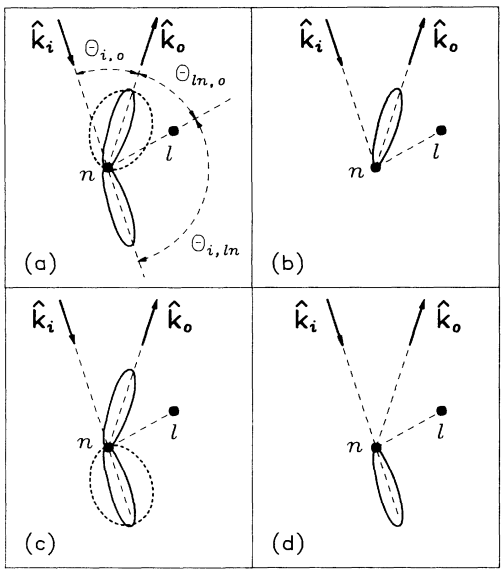

FIG. 4. (a) Polar plots of the DW factor $F_{nl}^{(1)}$, broken line, and of the product $f(\theta_{i,ln})f(\theta_{ln,o})$, full line. (b) Polar plot of the triple product $F_{nl}^{(1)}f(\theta_{i,ln})f(\theta_{ln,o})$. (c) Same as (a) but the broken line corresponds to $F_{nl}^{(2)}$. (d) Polar plot of the triple product $F_{nl}^{(2)}f(\theta_{i,ln})f(\theta_{ln,o})$. The origin of coordinates is at the atom position $\mathbf{R}_n$ and the polar variable is the angular position of the atom at $\mathbf{R}_l$. The products of the elastic scattering amplitudes have been normalized to unity along $\hat{\mathbf{k}}_i$ and $\hat{\mathbf{k}}_o$, and the DW factors have been computed with $\sigma^2=0.0065$ Å^2. The energy is $E=700$ eV.

Despite the great similarity between I_{inc} and I_{out}, there is a major difference in that the type of interferences which give rise to the term I_{inc} also appears in the description of XPD/AED and ARPEFS experiments, whereas I_{out} has no counterpart in such experiments. This connection with the physics of the diffraction of photoelectrons or Auger electrons was first pointed out by Egelhoff,[13] and has been used in the interpretation of several experiments.[6–8] However, a detailed analysis of how this connection comes about and to what extent it can be used to explain experiments has not been given yet. We will return to this point later in Sec. V.

IV. RESULTS

We will compare now some experimental and theoretical results obtained for the scattering of electrons from Cu(001) at room temperature. In spite of the very simple approximations made in the descriptions of the scattering process and of the thermal motion of the atoms, there is an overall good agreement which, besides confirming the general aspects of the theory, allows an analysis of the interplay of the different intensity terms. In particular we will stress those features of the experimental results which may be related directly to the hitherto not considered term I_{out}.

A. Calculation details

To compare the theory with the experiment we have to give values to $f(\theta)$, λ, and σ^2. The elastic scattering amplitude $f(\theta)$ was computed by the standard partial-wave method using the muffin-tin potential of Cu given by Moruzzi, Janak, and Williams.[14] The resulting scattering amplitudes are in good agreement with those used by other authors.[4,5] The electron mean free path and the mean squared displacement of the atoms were taken from the work of Kono *et al.*:[15] $\lambda=0.39$ Å$(E/\text{eV})^{1/2}$ and $\sigma^2=0.0065$ Å^2. We have also included the refraction of the electron at the surface by considering an inner potential $U_0=14.1$ eV.[15]

The summations of Eq. (7) were evaluated in the following way: in the summations over l, which converge rapidly, we considered only those second scatterers within a distance of 2.5 lattice constants of the first scatterer. The summations over n or n' were divided into a summation over the atoms in a layer, which can be made analytically, and a summation over layers, which was evaluated numerically. We have also integrated the intensities inside a cone of 6° half angle to simulate the angular acceptance of the analyzer. The angular convolutions of I_{dif}, I_{inc}, and I_{out} were made numerically using a nine-point grid, and that of I_{LEED} was made analytically assuming a δ-like angular dependence.

In an attempt to put the intensities on a common scale we have normalized the experimental intensities to that of a polycrystal and the theoretical results to $I_{\text{dif}}(T=\infty)$.[16]

B. Comparison of experiment and theory

Figure 5 presents the experimental results, in the form of polar intensity plots (PIP's), for the geometry depicted in Fig. 1. These results have been analyzed thoroughly in a previous publication.[8] The main features are the following: The PIP at 250 eV is dominated by LEED effects; the intense peak at $\theta_0 \approx 39°$ corresponds to the $(\bar{3}1)$ diffracted beam, and the other minor peaks correspond to the $(0\bar{2})$, $(\bar{1}\,\bar{1})$, $(\bar{2}0)$, and $(\bar{4}2)$ diffracted beams. Increasing the energy to 400 eV produces a decrease of the intensity of the LEED peaks, and the appearance of a broad structure at $\theta_0 \approx 45°$. A further increase of the energy to 800 eV makes the LEED peaks disappear completely, leaving a PIP similar to those observed in XPD/AED experiments:[17] two broad peaks at $\theta_0 = 0$ and 45° which correspond to exit directions along the internuclear axes [001] and [011], respectively, and a smaller structure at $\theta_0 \approx 20°$.

The calculated PIP's are shown in Fig. 6; in all the PIP's we have drawn the incoherent and the total intensities; the term I_{LEED} is the difference between these two curves. The PIP at 250 eV is in excellent agreement with the experiment; the incoherent intensity is small and, as expected, all the peaks belong to the term I_{LEED}. At 400 eV the main features are the loss of intensity of all the LEED peaks and the increase of some structures of the incoherent intensity, specially the one at $\theta_0 = 45°$, again in general agreement with the experiment. A discrepancy in the intensity of some individual LEED peaks will be explained below. Finally, at 800 eV all the LEED peaks have disappeared completely and the calculated PIP corresponds entirely to the incoherent intensity; as in the measured PIP, there are two big structures at $\theta_0 = 0$ and 45° and a smaller one at $\theta_0 \approx 20°$.

Therefore the theory predicts correctly that at an energy of ~400 eV the intensity of the elastically reflected electrons passes from a regime dominated by I_{LEED} to a regime dominated by the incoherent intensity $I_{\mathrm{inc}} + I_{\mathrm{out}} + I_{\mathrm{dif}}$. It is also seen that the incoherent intensity has many structures, similar to those observed in XPD/AED experiments, due to the terms I_{inc} and I_{out}.

Note that the good description of the transition between the two regimes has been obtained with no adjustable parameters. However, with the simple models we are using to describe the scattering process and the thermal motion of the atoms, some discrepancies with the experiment are unavoidable. Among them are the wrong intensities of the LEED peaks $(0\bar{3})$, $(\bar{1}\,\bar{2})$, and $(\bar{5}2)$ in the PIP at 400 eV, and the overestimate of the structures in the incoherent intensity. Figure 7 shows that the large intensity of the $(\bar{1}\,\bar{2})$ peak in the PIP of 400 eV is due to the occurrence of an intensity maximum in the *I-E* curve at exactly this energy, and that maxima of intensity of the diffracted beams $(0\bar{3})$ and $(\bar{5}2)$ occur slightly above 400 eV. Based on the results of Barton, Xu, and Van Hove,[5]

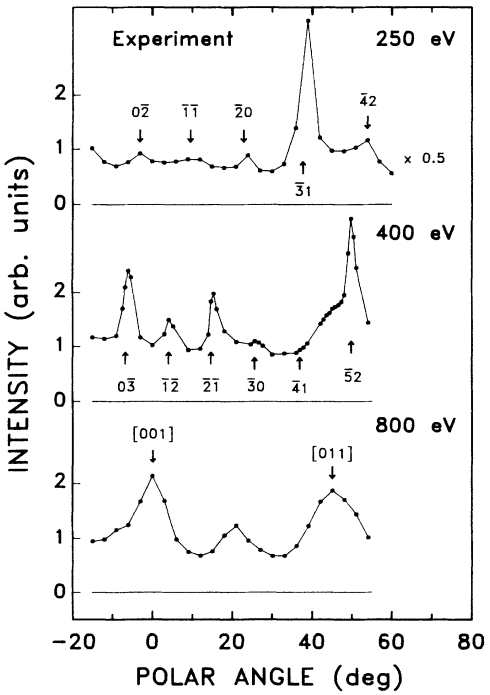

FIG. 5. Experimental polar intensity plots (PIP's) of the elastic reflection of electrons from Cu(001). The intensities have been normalized to the elastic reflection from polycrystalline Cu. The arrows indicate LEED directions in the PIP's of 250 and 400 eV, and crystallographic directions in the PIP of 800 eV. Note that the PIP of 250 eV has been multiplied by 0.5.

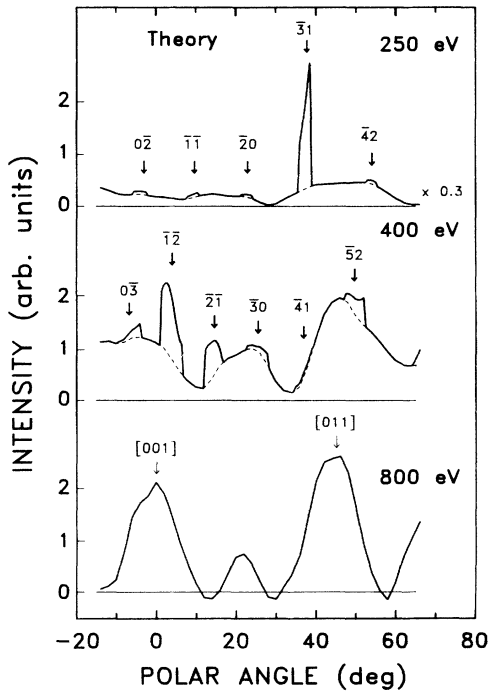

FIG. 6. Calculated PIP's of the elastic reflection of electrons from Cu(001). The intensities have been normalized to $I_{\mathrm{dif}}(T=\infty)$. The broken line corresponds to the *incoherent* intensity and the full line to the total intensity. Note that the PIP of 250 eV has been multiplied by 0.3.

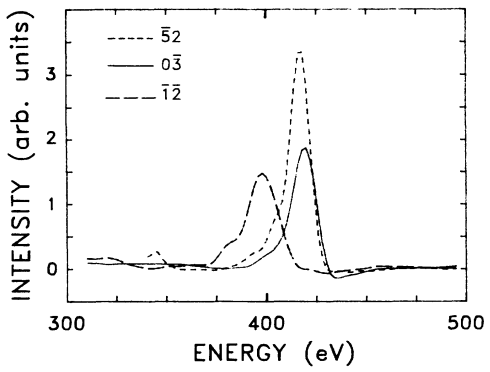

FIG. 7. Calculated intensity vs energy curves for the diffracted beams $(\bar{5}2)$, $(0\bar{3})$, and $(\bar{1}\,\bar{2})$ (Ref. 18).

we expect that the inclusion of higher-order interferences in I_{LEED} should shift these maxima towards lower energies, thereby producing in the PIP of 400 eV both a reduction of the intensity of the $(\bar{1}\,\bar{2})$ peak and an increase of the intensities of the $(0\bar{3})$ and $(\bar{5}2)$ peaks.

Figures 8–10 show experimental and calculated PIP's at energies at which the LEED peaks have disappeared completely. In the calculated PIP's we have also drawn the terms I_{inc} and I_{out}; the term I_{dif} is constant and amounts to nearly one in all the PIP's. The first thing to be noted is that the term I_{out} is never negligible; this is rather surprising if one thinks that the experimental geometry had been designed to emphasize interference effects in the outgoing part of the trajectory and to minimize them in the incoming part.[8] The I_{inc} curves have the three peaks at $\theta_0 \approx 0$, 20°, and 45° characteristic of XPD/AED PIP's. The I_{out} curves have also peaks at

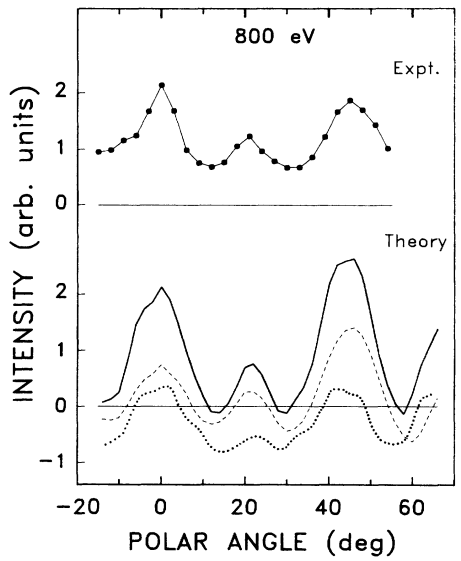

FIG. 8. Experimental and calculated PIP's of the elastic reflection of electrons at 800 eV. In the calculated PIP the solid line corresponds to the total intensity, the dashed line to the term I_{inc}, and the dotted line to the term I_{out}. The terms I_{dif} and I_{LEED} are nearly one and zero, respectively.

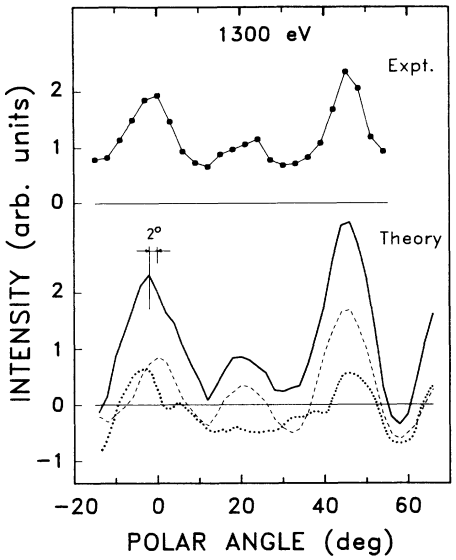

FIG. 9. Experimental and calculated PIP's of the elastic reflection of electrons at 1300 eV. In the calculated PIP the peak at $\theta_0 \approx 0$ has shifted towards negative angles.

$\theta_0 \approx 0$ and 45°, but take negative values at other angles. Since the magnitude of the negative values of I_{out} is almost as large as the term I_{dif}, there is a near cancellation of the terms that produces an apparent absence of background in the calculated PIP's. We expect that, as in XPD/AED and ARPEFS calculations, the inclusion of spherical-wave corrections[19] and multiple-scattering effects[20,21] will reduce the size of the modulations of I_{inc} and I_{out}, thereby bringing the theory into better agreement with the experiment. It is observed that the peak at $\theta_0 \approx 0$ in I_{out} shifts towards negative angles when the energy is increased, and that this eventually shifts the total

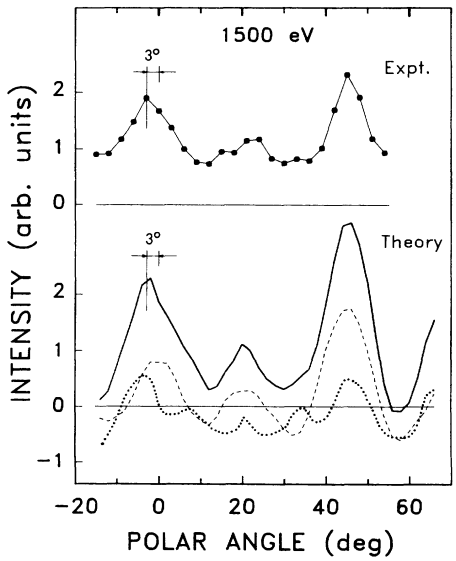

FIG. 10. Experimental and calculated PIP's of the elastic reflection of electrons at 1500 eV. In both PIP's the peak at $\theta_0 \approx 0$ has shifted towards negative angles.

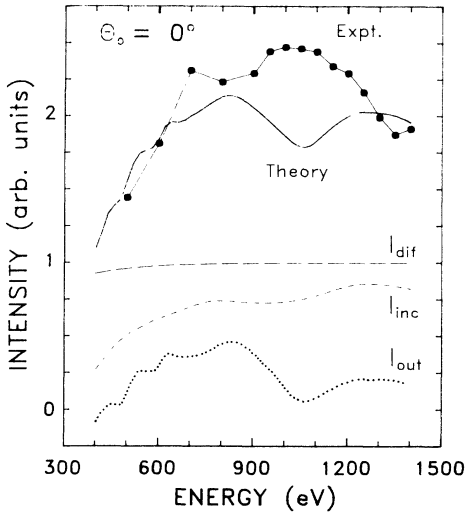

FIG. 11. Experimental and calculated intensities at $\theta_0=0$ as a function of the energy. The three components of the theoretical intensity are also shown.

intensity peak. This effect, corroborated by the experiment, illustrates the importance of the term I_{out}.

The energy dependences of the intensities at $\theta_0=0$ and 45° are shown in Figs. 11 and 12. It is seen that the trends of the experimental curves are reproduced remarkably well by the calculated curves. The magnitudes of the intensities seem to be correct at $\theta_0=0$ but too big at $\theta_0=45°$; however, it must be pointed out that a precise agreement is not to be expected in view of the different normalizations of the experimental and calculated intensities, and of the neglect of spherical-wave corrections and multiple-scattering effects in the calculation. Note that the marked threshold at ~400 eV of the intensity at $\theta_0=0$ is due to the fall in this region of both I_{inc} and I_{out}. On the contrary, at $\theta_0=45°$ the fall of I_{inc} is compensated by an increase of I_{out} below 600 eV; this compensation of the variations of I_{inc} and I_{out} causes the plateau observed in the experiment.

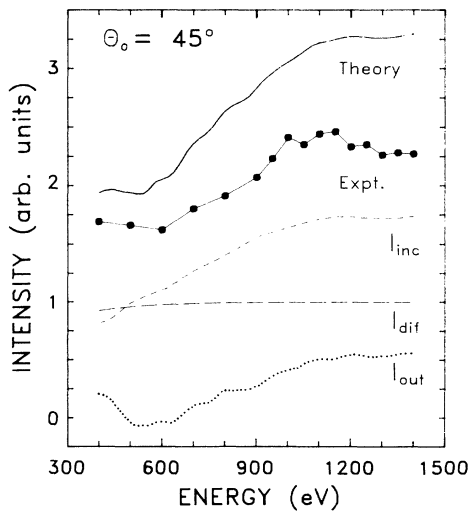

FIG. 12. Experimental and calculated intensities at $\theta_0=45°$ as a function of the energy.

V. DISCUSSION

We have shown in the preceding section that the results of the theory developed in Sec. III are in reasonably good agreement with the experiments. However, in our opinion the main achievement of the theory has been to connect two well-differentiated regimes of the elastic reflection of electrons from crystalline surfaces: the low-energy regime, in which the intensity is dominated by LEED effects, and the regime of intermediate energies, in which modulations like those observed in XPD/AED experiments are the dominant factor.

The passage from one regime to another is determined by the thermal vibration of the atoms. In the low-energy regime the thermal effects are of little importance and all the scattered waves add *coherently*; the DW factors are all near unity and the intensity is dominated by I_{LEED}. In the regime of intermediate energies the thermal disorder of the lattice becomes more important and destroys all the long-range coherency responsible for the LEED peaks; however, the interferences of the waves with the same *incoming or outgoing* paths are little affected by the temperature and come to dominate the intensity through the terms I_{inc} and I_{out}.

The elastic reflection of electrons in the LEED regime is one of the most well-studied problems in surface science and need not be analyzed here. On the contrary, the regime of intermediate energies has received much less attention; the patterns observed at these energies have been generally interpreted as due to quasielastic or Kikuchi electrons,[22–24,7] assuming a two-step process: (i) inelastic and incoherent scattering of the incident electron at a lattice site (involving an energy loss so small that the electron is practically indistinguishable from the truly elastic electrons), and (ii) diffraction of the electron on its way to the surface. We have proved that the inelastic scattering of the electron is not a *necessary* prerequisite, since as shown in Sec. III, the thermal disorder of the lattice also makes the *elastic* electrons to produce a similar pattern. Regarding the diffraction of the electron, in former papers it was assumed that the structures were part of Kikuchi bands,[22–24] which originate in Bragg reflections in the atomic planes and therefore are a volume effect, whereas in more recent papers a cluster-type model like the one used here was adopted.[6,7] Although we have not made a detailed comparison of the two diffraction models, we think that any structure due to Kikuchi bands, if present, must be very small; this is based on the results of Trehan, Osterwalder, and Fadley,[25] and on our own observation that complete convergence of the numerical results occurred in all cases for 7–10 layers, which is barely the minimum degree of periodicity necessary for the Kikuchi bands to develop.

We think that the theory presented in this work provides the correct framework in which the problem of the elastic reflection of electrons should be treated. The different contributions to the intensity as well as the ap-

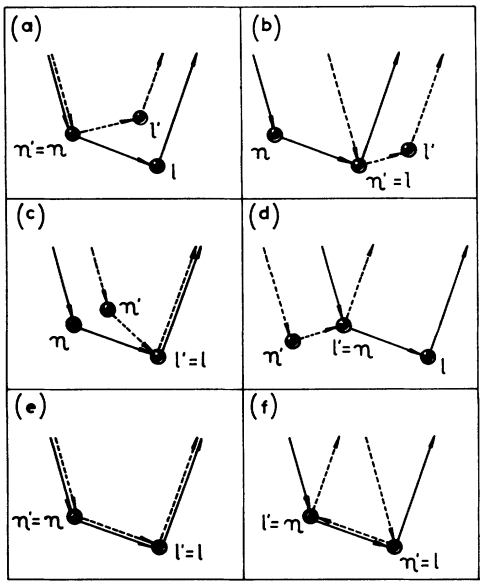

FIG. 13. Schematic representation of the new types of interferences which must be considered when the interference between DSW's is included in Eq. (2).

proximations that can be made appear naturally, and the transition from one type of pattern to the other can be explained without need of *ad hoc* assumptions. The results shown in the preceding section correspond to the theory in its simplest version, and thus the agreement with the experiment is not the best. In its present state the theory is equivalent to the plane-wave single-scattering theories of XPD/AED and ARPEFS; to make it capable of more accurate quantitative predictions one must include spherical-wave[19] and multiple-scattering corrections,[20,21] which are known to produce a reduction of the intensity modulations, specially in those cases in which forward scattering is important. Formally, the spherical-wave corrections involve only a redefinition of the scattering amplitudes, but the numerical calculation can become more cumbersome. Multiple-scattering corrections are easily introduced by allowing more terms in Eq. (2). Note that an important consequence of this will be the appearance of new terms in the *incoherent* intensity that will not fit in I_{dif}, I_{inc}, or I_{out}. For example, if we had included in Eq. (2) the interference between DSW's, we would have had contributions to the *incoherent* intensity from the six types of waves represented in Fig. 13. The interferences of waves of types (a), (c), and (e) would have been included into I_{inc}, I_{out}, and I_{dif}, respectively, but the interferences of waves of types (b), (d), and (f) would have required the definition of entirely new terms.

Finally, if one wants to analyze extended fine-structure effects,[26] the model of *uncorrelated* atomic vibrations may become inappropriate, and a model which considers the *correlated* motion of neighboring atoms may be necessary.

VI. SUMMARY

By including thermal effects in a cluster-type theory of LEED we have obtained a theory that contains both the LEED effects at low energies and XPD/AED effects at intermediate energies. It has been shown that the interferences between waves that share part of their paths inside the solid are less affected by the temperature than the interferences between waves with no point of contact; thus these interferences survive the fall off of the long-range coherency at intermediate energies and give rise to the structures of the type of XPD/AED experiments.

The comparison with the experiment has shown that (i) the theory predicts correctly the transition from one regime to the other at an energy of ~400 eV; (ii) there is a good qualitative agreement; (iii) a good quantitative agreement must await the incorporation in the theory of spherical-wave corrections, multiple scattering, and correlated atomic vibrations.

ACKNOWLEDGMENTS

R.O.B. and G.Z. are also members of the Consejo Nacional de Investigaciones Científicas y Técnicas (CONICET). H.A. would like to thank CONICET and R.O.B. would like to thank Fundación Antorchas for financial support.

[1]W. F. Egelhoff, Crit. Rev. Solid State Mater. Sci. **16**, 213 (1990).
[2]C. S. Fadley, in *Synchrotron Radiation Research: Advances in Surface Science*, edited by R. Z. Bachrach (Plenum, New York, 1990).
[3]J. J. Barton, S. W. Robey, and D. A. Shirley, Phys. Rev. B **34**, 778 (1986).
[4]M. Sagurton, E. L. Bullock, and C. S. Fadley, Surf. Sci. **182**, 287 (1987).
[5]J. J. Barton, M.-L. Xu, and M. A. Van Hove, Phys. Rev. B **37**, 10475 (1988).
[6]S. A. Chambers, I. M. Vitomirov, S. B. Anderson, and J. H. Weaver, Phys. Rev. B **35**, 2490 (1987); S. A. Chambers, I. M. Vitomirov, and J. H. Weaver, *ibid.* **36**, 3007 (1987).
[7]H. Cronacher, K. Heinz, K. Müller, M.-L. Xu, and M. A. Van Hove, Surf. Sci. **209**, 387 (1989).
[8]H. Ascolani, M. M. Guraya, and G. Zampieri, Phys. Rev. B **43**, 5135 (1991).
[9]P. A. Lee and J. B. Pendry, Phys. Rev. B **11**, 2795 (1975).
[10]J. B. Pendry, *Low-Energy Electron Diffraction* (Academic, London, 1974).
[11]N. D. Mermin, J. Math. Phys. **7**, 1038 (1966).
[12]In a more general formulation I_{dif} must include also the square modulus of each multiply scattered wave.
[13]W. F. Egelhoff, J. Vac. Sci. Technol. A **4**, 758 (1986).
[14]V. L. Moruzzi, J. F. Janak, and A. R. Williams, *Calculated Electronic Properties of Metals* (Pergamon, New York, 1978).
[15]S. Kono, S. M. Goldberg, N. F. T. Hall, and C. S. Fadley, Phys. Rev. B **22**, 6085 (1980).
[16]This gives the dispersion of the incident beam by a collection of atoms with random positions.
[17]W. F. Egelhoff, Phys. Rev. B **30**, 1052 (1984); H. Li and B. P.

Tonner, *ibid.* **37**, 3959 (1988).

[18]In the geometry of our experiment (see Fig. 1), both the exit and the incident directions vary during the scan of a PIP. Therefore the *I-E* curves of the $(\bar{5}2)$, $(0\bar{3})$, and $(\bar{1}\,\bar{2})$ diffracted beams have been computed for the incident directions corresponding to the exit directions with angles $\theta_0 = -4°$, 3°, and 52°, respectively. The incident directions are $\epsilon_i = 47°$, $\phi_i = 47°$ for the $(\bar{5}2)$ beam, $\epsilon_i = 52°$, $\phi_i = 125°$ for the $(0\bar{3})$ beam, and $\epsilon_i = 56°$, $\phi_i = 117°$ for the $(\bar{1}\,\bar{2})$ beam, where ϵ_i are the elevation angles as defined in Fig. 1 and ϕ_i the azimuthal angles measured from the [010] axis. Note that the diffracted beams enter the analyzer *only* at 400 eV.

[19]J. J. Barton and D. A. Shirley, Phys. Rev. B **32**, 1892 (1985); J. Mustre de Leon, J. J. Rehr, C. R. Natoli, C. S. Fadley, and J. Osterwalder, *ibid.* **39**, 5632 (1989).

[20]S. Y. Tong, H. C. Poon, and D. R. Snider, Phys. Rev. B **32**, 2096 (1985).

[21]M.-L. Xu, J. J. Barton, and M. A. Van Hove, Phys. Rev. B **39**, 8275 (1989); M.-L. Xu and M. A. Van Hove, Surf. Sci. **207**, 215 (1989).

[22]A. Mosser, Ch. Burggraf, S. Goldsztaub, and Y. H. Ohtsuki, Surf. Sci. **54**, 580 (1976).

[23]H. Hilferink, E. Lang, and K. Heinz, Surf. Sci. **93**, 398 (1980).

[24]M. V. Gomoyunova, I. I. Pronin, and I. A. Shmulevitch, Surf. Sci. **139**, 443 (1984).

[25]R. Trehan, J. Osterwalder, and C. S. Fadley, J. Electron Spectrosc. Relat. Phenom. **42**, 187 (1987).

[26]As in ARPEFS, if one varies the energy of the electrons, keeping constant the incoming and the outgoing directions, the terms I_{inc} and I_{out} may present fine-structure modulations.